Human Genetic Polymorphisms in T1R1 and T1R3 Taste Receptor Subunits Affect Their Function

Mariam Raliou[1], Marta Grauso[1], Brice Hoffmann[1], Claire Schlegel–Le-Poupon[1], Claude Nespoulous[1], Hélène Débat[1,3], Christine Belloir[2], Anna Wiencis[2], Maud Sigoillot, Singh Preet Bano[3], Didier Trotier[4], Jean-Claude Pernollet[1], Jean-Pierre Montmayeur[2], Annick Faurion[4] and Loïc Briand[2]

[1]Institut National de la Recherche Agronomique, Unité Mixte de Recherche 1197 Neurobiologie de l'Olfaction et de la Prise Alimentaire—Biochimie de l'Olfaction et de la Gustation, Domaine de Vilvert, F-78350, Jouy-en-Josas, France, [2]Centre des Sciences du Goût et de l'Alimentation, Unité Mixte de Recherche 6265 CNRS, Unité Mixte de Recherche 1324 Institut National de la Recherche Agronomique, Université de Bourgogne, Agrosup Dijon, F-21000, Dijon, France, [3]Université Versailles St-Quentin, 45 avenue des Etats-Unis, F-78035, Versailles, France and [4]Institut National de la Recherche Agronomique, Unité Mixte de Recherche 1197 Neurobiologie de l'Olfaction et de la Prise Alimentaire—Neurobiologie Sensorielle, Domaine de Vilvert, F-78350, Jouy-en-Josas, France

Correspondence to be sent to: Loïc Briand, Centre des Sciences du Goût et de l'Alimentation, Unité Mixte de Recherche 6265 CNRS, Unité Mixte de Recherche 1324 Institut National de la Recherche Agronomique, Université de Bourgogne, Agrosup Dijon, F-21000, Dijon, France. e-mail: loic.briand@dijon.inra.fr

Accepted February 3, 2011

Abstract

Umami is the typical taste induced by monosodium glutamate (MSG), which is thought to be detected by the heterodimeric G protein–coupled receptor, T1R1 and T1R3. Previously, we showed that MSG detection thresholds differ substantially between individuals and we further showed that nontaster and hypotaster subjects are associated with nonsynonymous single polymorphisms occurring in the T1R1 and T1R3 genes. Here, we show using functional expression that both amino acid substitutions (A110V and R507Q) in the N-terminal ligand-binding domain of T1R1 and the 2 other ones (F749S and R757C), located in the transmembrane domain of T1R3, severely impair in vitro T1R1/T1R3 response to MSG. A molecular model of the ligand-binding region of T1R1/T1R3 provides a mechanistic explanation supporting functional expression data. The data presented here support causal relations between the genotype and previous in vivo psychophysical studies in human evaluating sensitivity to MSG.

Key words: human, ʟ-glutamate, MSG, SNP, taste receptors, T1R1/T1R3, umami

Introduction

Umami is the typical taste induced by monosodium glutamate (MSG) found naturally in many protein-rich foods, such as seafoods, meat, and cheese and certain fruit and vegetables. The most unique feature of umami taste is its potentiation by purine nucleotides inosine-5′-monophosphate (IMP) and guanosine-5′-monophosphate (GMP), which also elicit umami taste on their own (Kuninaka 1960; Kuninaka et al. 1964; Yamaguchi 1991). The detection of glutamate in taste cells is considered to involve G protein–coupled receptors (GPCRs). Metabo-tropic glutamate receptors types 1 and 4 and their truncated forms namely taste-mGluR1 (Toyono et al. 2002; San Gabriel et al. 2005, 2009) and taste-mGluR4 (Chaudhari et al. 1996; Yang et al. 1999; Chaudhari et al. 2000) are found in taste buds of mice and rats. However, taste-mGluRs are activated by glutamate and analogs but are not reported to be sensitive to ribonucleotides. There is good evidence that the T1R1 (taste receptor type 1, member 1, *tas1r1*) and T1R3 (taste receptor type 1, member 3, *tas1r3*) GPCR heterodimer is involved in umami taste perception in

rodents and humans, whereas T1R2 (taste receptor type 1, member 2, *tas1r2*) and T1R3 assemble to form a taste receptor sensitive to several sweet taste eliciting chemicals (Nelson et al. 2001, 2002; Li et al. 2002). Functional expression assays in HEK293 cells have demonstrated that rodent and human T1R1/T1R3 are activated by L-glutamate with responses enhanced by the presence of IMP (Nelson et al. 2001, 2002; Li et al. 2002; Zhao et al. 2003), and the molecular mechanism of synergy between L-glutamate and IMP at the molecular level has been recently described (Zhang et al. 2008). Lactisole, a potent sweetness inhibitor, which binds human T1R3 is able to inhibit umami taste as well (Galindo-Cuspinera and Breslin 2006). However, with regard to mouse studies, the results obtained from mice with T1R3 knockout (T1R3-KO) are controversial. One study showed that for T1R3-KO mice, both behavioral preference and neural responses to MSG in the chorda tympani nerve—which innervates the anterior tongue—were totally absent (Zhao et al. 2003). These results indicated that T1R1/T1R3 is essential for MSG detection and perception in mice. In contrast, another study showed that a behavioral preference for MSG was reduced but not abolished in T1R3-KO mice (Damak et al. 2003), suggesting the existence of more than one receptor for umami taste in mice. Additional umami receptors have been also proposed (Maruyama et al. 2006; Chaudhari et al. 2009).

It is known that both in hamsters and humans, there is substantial interindividual taste sensitivity variability. For instance, detection thresholds for MSG have been reported to follow a multimodal distribution in the French population, with 2% of the population displaying a specific inability to taste MSG (Lugaz et al. 2002). Genetic factors affecting taste receptors have been shown to play a role in interstrain variability of sensitivity to tastants in mice and interindividual difference of sensitivity to tastants in humans. For example, saccharin preference in mice differs between inbred strains (Fuller 1974; Lush 1989) and is associated with nonsynonymous single polymorphisms (nsSNPs) in the T1R3 gene (Reed et al. 2004). In human, it is now established that taste variation in the bitter taste of propylthiouracil and phenylthiocarbamide is correlated to specific variants of the T2R38 taste receptor (Drayna et al. 2003; Bufe et al. 2005). We and others have reported nsSNP in the coding region of the human T1R1 and T1R3 genes (Kim et al. 2006; Raliou, Boucher, et al. 2009; Shigemura, Shirosaki, Ohkuri, et al. 2009). Some of them were demonstrated to be associated to the inability to taste MSG in nontasters and hypotasters in Caucasian French subjects (Raliou, Wiencis, et al. 2009), in Japanese (Shigemura, Shirosaki, Sanematsu, et al. 2009), and American populations (Chen et al. 2009). Raliou, Wiencis, et al. (2009) furthermore showed polymorphisms in mGluR1 contributed to explain the lack of sensitivity to MSG.

Earlier, we reported that T1R1 and T1R3 were found in human fungiform papillae of MSG tasters and nontasters and that some nsSNPs in the genes coding for the T1R1 and T1R3 receptors were correlated with lower detection thresholds for MSG in a sample of French population (Raliou, Wiencis, et al. 2009). These nsSNPs are listed in Table 1. Two of the 3 nsSNPs observed in T1R1 in our population sample (Raliou, Boucher, et al. 2009) occur in the Venus fly trap (VFT) domain, at amino acid positions 110 (SNP C329T) and 372 (SNP G1114A), leading to T1R1 variants T1R1-110V and T1R1-372T, respectively. The third nsSNP is located in the N-terminal part of the cysteine-rich region (CRR) at position 507 (SNP G1520A) leading to variant T1R1-507Q (Figure 1). In T1R3, we reported nsSNPs at amino acid 749 (SNP T2246C) and 757 (SNP C2269T) leading to variants T1R3-749S and T1R3-757C, respectively, all of them located in the heptahelical transmembrane domain (HTD) (Figure 1). We refer to the most common allele of these receptor subunits as T1R1 and T1R3.

In the present work, we functionally expressed these taste receptor variants the prevalence of which is sufficient for statistical evaluation (Raliou, Wiencis, et al. 2009). We analyzed their cellular response using an in vitro cellular assay followed by molecular modeling. We demonstrated that some receptor nsSNPs directly affect the function of the receptor in a manner that confirms earlier genotype–phenotype relationship studies.

Material and methods

Preparation of chimeric Gα16 and T1R expression constructs

Chimeric Gα mutant proteins as promiscuous G16Gust44 and G16Gi3 are widely used in the functional expression of taste T1R receptors (Li et al. 2002; Zhang et al. 2008). The first one (G16Gust44) was generated by replacing the C-terminus of Gα16 with the C-terminal 44 residues of gustducin and the other one (G16Gi3) by replacing the last 5 residues of the C-terminal tail of Gα16 (EINLL) by its counterpart from Gαi3 (ECGLY). The both constructs were generated by polymerase chain reaction (PCR) and cloned in pcDNA3.1/Hygro vector (Invitrogen). When we functionally expressed T1R1/T1R3 together with G16Gust44 or G16Gi3, we observed that cells responded to the same extend to MSG. However, we observed that G16Gi3 gave more reproducible calcium responses to MSG. We then used this chimera for this study. Human T1R1 was amplified from human fungiform papillae cDNA, whereas T1R2 and T1R3 were amplified from human genomic DNA and assembled using overlapping primers. The open reading frames of T1R1 and T1R2 were cloned into pcDNA3, whereas T1R3 was inserted in pcDNA4-myc-HisA (Invitrogen), generating pcDNA3-T1R1, pcDNA3-T1R2, and pcDNA4-T1R3 plasmids. T1R1 and T1R3 variants were generated through the subsequent introduction of point mutations using PCR-based direct mutagenesis (QuikChange Multi Site-Directed

Table 1 Table recapitulating the nature and location of the *Tas1r1* and *Tas1r3* cSNPs studied

Gene (Gban)	Position of cSNP (nt)	Allele	Exon	rs #	Position in protein (aa)	Amino acid encoded	Localization in receptor	Allele frequency
Tas1r1 (BC136516)	329	C	2	41278020	110	Alanine (A)	VFT	0.98
		T				Valine (V)		0.02
	1114	G	3	34160967	372	Alanine (A)	VFT	0.80
		A				Threonine (T)		0.20
	1520	G	5	35118458	507	Arginine (R)	CRR	0.975
		A				Glutamine (Q)		0.025
Tas1r3 (BC152912)	2246	T	6	79148073	749	Phenylalanine (F)	TM5	0.99
		C				Serine (S)		0.01
	2269	C	6	307377	757	Arginine (R)	ICL3	0.985
		T				Cysteine (C)		0.015

VFT, Venus fly trap domain; CRR, cysteine-rich region; TM5, transmembrane domain 5; ICL3, Intracellular loop 3; TM5 and ICL3 are part of the transmembrane domain region; nt, nucleotides; rs#, rs number; aa, amino acid; Gban, Genbank accession number.
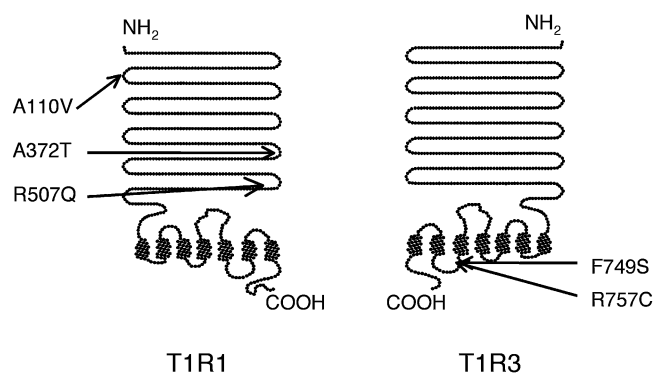
Figure 1 T1R1 and T1R3 snake representation with location of amino acid variations listed in Table 1.

Mutagenesis Kit, Stratagene). The integrity of all constructs was checked by automated DNA sequencing.

Functional expression and calcium imaging

HEK293 cells were grown in Minimal Essential Medium without phenol red (GIBCO, Invitrogen) supplemented with 10% heat-inactivated fetal bovine serum (FBS) (Hyclone, Perbio), 2 mM L-glutamine (GIBCO), and Eagle's nonessential amino acids (Eurobio) and maintained at 37 °C in a humidified incubator with 5% CO_2. Then cells were transfected with pcDNA3.1/Hygro/G16Gi3 plasmid using Lipofectamine2000 (Invitrogen) according to the manufacturer's instructions. HEK293 derivative cells stably expressing G16Gi3 (HEK293/G16Gi3) were selected in 300 μg/mL hygromycin B (Invitrogen) amplified and frozen in several cryovials in order to use the same batch of cells over the course of the study.

T1R1 or T1R3 and their variants were transiently cotransfected in HEK293/G16Gi3 cells using 3 μg of plasmid DNA (1.5 μg of T1R plasmid and 1.5 μg of pUC18) using JetPEI (PolyPlus Transfection; Ozyme). After 24 h, transfected cells were trypsinized and seeded at a density of $0.7\ 10^5$ cells per well onto a poly-L-lysine–coated 96-well tissue culture plate (black 96-well Microplate with clear bottom, Greiner Bio-one) and grown in low-glucose DMEM (Dulbecco's Modified Eagle's Medium, GIBCO; Invitrogen) supplemented with 10^{-6} mM GlutaMAX and 10% dialyzed FBS in order to minimize glutamate-induced and glucose-induced desensitization.

After 24 h, transfected cells were rinsed twice with calcium assay buffer (Hank's *N*-2-hydroxyethylpiperazine-*N'*-2-ethanesulfonic acid [HEPES] balanced salt solution supplemented with HEPES 20 mM buffered pH 7.2) and loaded 30 min at 37 °C with Fluo-4 acetoxymethyl ester dye (3.5 μM) (Molecular Probes) dissolved in calcium assay buffer supplemented with 0.025% (w/v) pluronic acid (Molecular Probes) and 0.1% (w/v) bovine serum albumin (BSA). Then cells were rinsed twice with calcium assay buffer and incubated in it for 10 min at 37 °C and 1.25 h in the dark at 25 °C. The cells were stimulated by the addition of MSG (Ajinomoto Eurolysine) using a micropipette. At the end of the experiment, isoproterenol (0.5 μM) was applied as a control to stimulate the endogenously expressed β2-adrenergic receptors. Calcium imaging was monitored on an inverted epifluorescence microscope (CK40, Olympus) equipped with a digital camera (ORCA-ER; Hamamatsu Photonics). Calcium responses (485 nm excitation and 535 nm emission wavelengths) were recorded each second during 2 min after stimuli addition using a binning 2×2. The data were then normalized to isoproterenol calcium responses by dividing the peak value of the MSG response by the peak value of the isoproterenol response for each cell and analyzed using SimplePCI software (Hamamatsu,

Compix). The Ca^{2+} changes were expressed as fractional change in fluorescence light intensity: F/F = (F – F0)/F0, where F is the fluorescence light intensity at each point and F0 is the value of emitted fluorescent light before the stimulus application. Data were compiled from 100 cells and represented as averaged maximal fluorescence increase of at least 5 independent experiments carried out in triplicate. Dose–response curves were fitted using SigmaPlot software (Integral Software).

Polyclonal T1R1–specific antibody production and western blot analysis

Antibodies against hT1R1 were generated by Eurogentec Ltd. Briefly, the VFT domain of T1R1 (T1R1-VFT) corresponding to residues F21–S495 of the human receptor was expressed in *Esherichia coli* as inclusion bodies. Inclusion bodies were washed and solubilized using 6 M guanidium chloride. The pure protein T1R1-VFT was refolded using dialysis and used for the production of rabbit polyclonal antibodies. Details of the expression and refolding of T1R1-VFT will be published elsewhere. As a control for the specificity of the interactions, T1R2-VFT and T1R3-VFT (amino acids A22-S493 and A21-S497, respectively) were similarly produced and refolded. Anti-T1R3-VFT antibodies were obtained from Novus Biologicals (NLS 5060; Interchim). For immunoblotting of T1Rs-VFT, 30 ng of protein/lane were fractionated by 10% acrylamide sodium dodecyl sulfate–polyacrylamide gel electrophoresis (SDS–PAGE) and transferred to polyvinylidene fluoride membrane. The blot was blocked with 5% (w/v) skim milk in saline Tris buffer pH 7.5 containing 0.05% Tween 20, then incubated with crude antiserum at 1/1000 dilution. Subsequently, the membrane was incubated with a secondary goat anti-rabbit antibody conjugated to horseradish peroxidase (Biorad) at a dilution of 1/50 000. T1Rs-VFT proteins were detected with an enhanced chemiluminescence system (Biorad).

Immunohistochemistry

Immunohistostaining was performed as described by Bufe et al. (2005). Briefly, HEK293/G16Gi3 stable cells were seeded on 4-well culture slides (BD Biosciences) and transiently transfected with T1R1, T1R2, and T1R3 or their variants, using FuGENE HD (Promega). After 48 h, cells were rinsed twice with Hank's HEPES balanced salt solution and cooled on ice for 1 h. For the colocalization of the receptors with the plasma membrane, cells were incubated on ice with 20 µg/mL biotine–concanavalin A for 1 h and permeabilized for 5 min in acetone–methanol (1:1). Cells were blocked in 10% BSA in phosphate-buffered saline (PBS) for 30 min at 25 °C and incubated for 1 h at 25 °C with the primary antibodies anti-T1R1 or anti-T1R3 (NLS 5060; Novus Biologicals, Interchim) diluted respectively at 1/400 and 1/100 in Dako Antibody diluent (Dako). The plasma membrane was visualized with avidin D-tetramethyl rhoda-

mine isothiocyanate (TRITC) (1/200; Vector Laboratories, AbCys, France). Cells were then rinsed twice with PBS for 5 min and incubated with the secondary antibody Alexa Fluor 488 donkey anti-rabbit IgG (Invitrogen), diluted at 1/400 in Dako Antibody diluent for 1 h at 25 °C to visualize the receptors. After washing the cells with PBS, nuclei were stained with 49,6-diamidino-2-phenylindole (DAPI)–HCl present in the mounting medium (ProLong Gold antifade reagent; Molecular probes). The cells were analyzed using a confocal microscope (Leica TCS SP2 AOBS; DimaCell confocal facilities, Institut National de la Recherche Agronomique Dijon). To determine the expression rates, an identical protocol was used except that concanavalin A and avidin D-TRITC were omitted during the staining procedure. The cells were analyzed using a fluorescent microscope (TiE; Nikon) equipped with a LucaR EMCCD Camera (Andor Technology).

Molecular modeling and L-glutamate docking

A homology model of T1R1/T1R3 VFT (closed-open form/ A form) was performed by MODELLER (Sali and Blundell 1993) using the crystal structure of mGluR1 VFT (PDB accession number 1EWK) as template. Three servers, LALIGN (Huang et al. 1990), FUGUE (Shi et al. 2001), and NPS@ (Combet et al. 2000), were used to generate the sequence alignment. The model with the lowest energy was selected and validated using PROCHECK (Laskowski et al. 1996). Energy minimization was performed using NAMD2.5 program (Phillips et al. 2005) using Charmm27 topology parameters. The model was visualized using VMD2.6 software (Humphrey et al. 1996). AutoDockTools 1.5.2 (Sanner 2005) was used to add polar hydrogens and assign Gasteiger charges to the structure model and L-glutamate. Autogrid4 was used to create affinity grids centered on the potential active site located between lobes LB1 and LB2 in T1R1. Autodock4 with Lamarckian genetic algorithm was used to simulate ligand-receptor docking. Docking parameters were chosen using population size of 150, number of energy evaluation of 25 000 000 and 500 runs. Docked conformations were clustered using external clustering script provided with AutoDockTools 1.5.2. Reported docking results correspond to the lowest relative binding energy (sum of intermolecular energy and torsional free-energy penalty in kilocalorie per mole) of the most populated cluster and the root mean square deviations (RMSDs) of the ligand positions.

Results

Previously, we showed that MSG detection thresholds differ substantially between individuals and that the nontaster trait is associated with nsSNPs occurring in the T1R1 and T1R3 genes (Table 1 and Figure 1). To evaluate the impact of amino acid variation on receptor function, we cloned
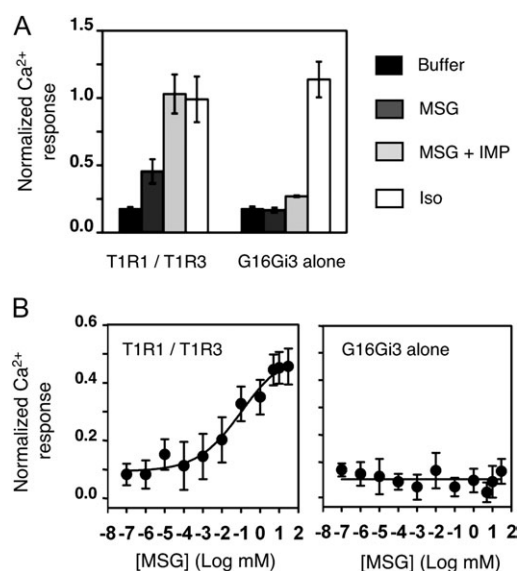
Figure 2 **(A)** Increases in the calcium concentrations in HEK293 cells transfected with G16Gi3, human T1R1 and T1R3 after stimulation with various stimuli. Cells coexpressing G16Gi3, human T1R1 and T1R3 responded to MSG (5 mM), and IMP (0.5 mM) potentiated the T1R1/T1R3 response to MSG. Isoproterenol (Iso; 0.5 μM), which activates endogeneous β2-adrenergic receptor, was used as a positive control. In absence of T1R1/T1R3 receptor, no obvious calcium responses were observed in the cells. **(B)** Dose–response relationship of cells cotransfected with T1R1/T1R3 or mock-transfected cells (cells expressing G16Gi3 alone) after stimulation with increasing concentration of MSG. No obvious calcium response was observed in cells in the absence of T1R1/T1R3. Amplitudes of MSG responses have been normalized to those induced by 0.5 μM isoproterenol. Each point represents the mean and the standard error of the mean of at least 5 independent experiments carried out in triplicate. Data were fitted with sigmoid dose–response curves using SigmaPlot software.

the coding sequence of T1R1 and T1R3, generated the previously observed receptor variants using site-directed mutagenesis and functionally expressed them into HEK293 cells stably expressing G16Gi3. We then monitored activation using calcium imaging. Cells coexpressing G16Gi3, human T1R1 and T1R3 responded to 5 mM MSG (Figure 2A), whereas cells expressing only G16Gi3 showed no calcium response. Isoproterenol, which activates endogenous β2-adrenergic receptor was used for data normalization. We found that isoproterenol signals are not influenced by the MSG stimulus. We observed a synergism (Figure 2A) between MSG and the 5′-ribonucleotide IMP, which is the hallmark of umami taste (Kuninaka 1960; Kuninaka et al. 1964; Yamaguchi 1991) thus pointing to a specific response to MSG in these cells.

   Calcium responses of receptor-expressing cells were monitored when exposed to different concentrations of MSG. MSG elicited transient intracellular calcium increases in G16Gi3 cells cotransfected with T1R1 and T1R3, in a concentration-dependent manner (Figure 2B) leading to a half-maximal response (EC_{50}) value of 0.17 ± 0.11 mM. This value is lower than the EC_{50} value reported by Shigemura, Shirosaki, Sanematsu, et al. (2009) for T1R1/
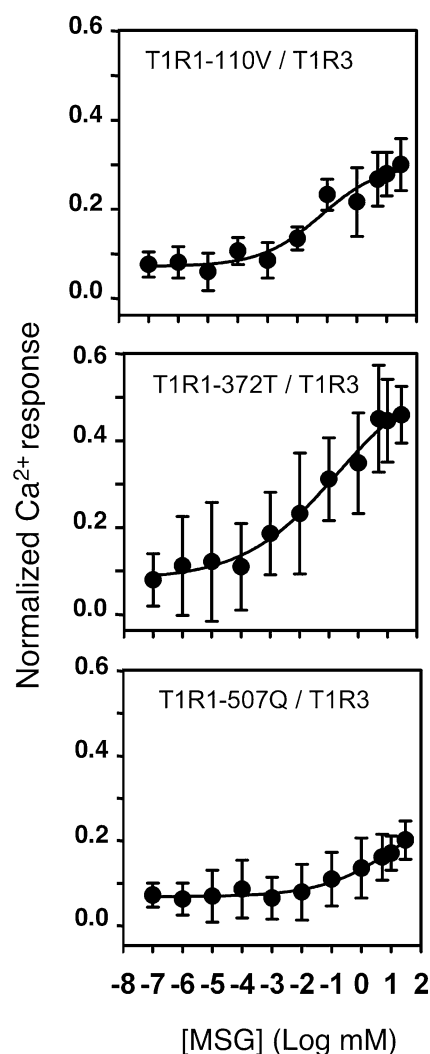

Figure 3 Dose–response relationship of cells cotransfected with T1R1 variants and T1R3. Amplitudes of MSG responses have been normalized to those induced by isoproterenol (0.5 μM), which activates endogenous β2-adrenergic receptor. Each point represents the mean and the standard error of the mean of at least 5 independent experiments carried out in triplicate. Data were fitted with sigmoid dose–response curves using SigmaPlot software.

T1R3 (27.6 mM). This discrepancy of MSG potency could be explained by a varying degree of cell surface expression of T1R1/T1R3 receptor due to different experimental procedures such as vector constructions, cell transfection efficiencies, or cell culture conditions. As a control, cells expressing G16Gi3 alone did not elicit any transient intracellular calcium increase (Figure 2B) in the range of tested concentrations. At higher concentration (above 30 mM), we observed that MSG induced osmotic stress responses (data not shown). We then investigated the capacity of 3 T1R1 receptor variants to be activated by MSG. As shown in Figure 3, T1R1-110V/T1R3 and T1R1-507Q/T1R3 responded to MSG but were activated to approximately 50% and 25% of the T1R1/T1R3 response with EC_{50} values
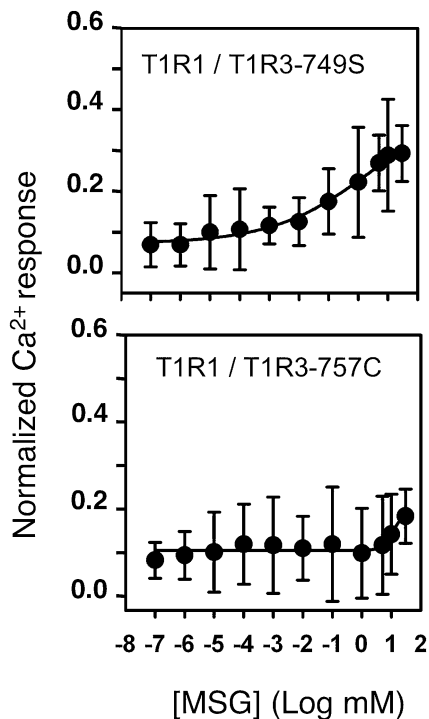
Figure 4 Dose–response relationship of cells cotransfected with T1R3 variants and T1R1. Amplitudes of MSG responses have been normalized to those of induced by isoproterenol (0.5 µM), which activates endogeneous β2-adrenergic receptor. Each point represents the mean and the standard error of the mean of at least 5 independent experiments carried out in triplicate. Data were fitted with sigmoid dose–response curves using SigmaPlot software.

Figure 5 Validation of rabbit polyclonal antibodies against T1R1-VFT and T1R3-VFT. Western blot analysis of T1Rs-VFT expressed in bacteria. T1R1-VFT, T1R2-VFT, and T1R3-VFT (30 ng of protein/lane) were separated by SDS–PAGE and visualized by immunoblotting using polyclonal anti-T1R1-VFT **(A)** or anti-T1R3-VFT **(B)** antibodies. (A) T1R1-VFT was detected, whereas T1R2-VFT and T1R3-VFT showed no signal. Molecular weight values are indicated. (B) T1R3-VFT was detected, whereas T1R1-VFT and T1R2-VFT showed no signal. Molecular weight values are indicated. **(C)** Immunocytochemistry of HEK293/G16Gi3 cells expressing T1R1/T1R3, T1R2/T1R3, T1R3, or mock-transfected cells (control). The T1Rs-expressing cells are shown in green, and nuclei are counterstained with DAPI (blue). The receptors were detected using polyclonal anti-T1R1 antibodies and fluorescently labeled by a secondary Alexa-488–conjugated antibody. All data were obtained from the same transfection experiment. HEK293/G16Gi3 cells in the absence of T1R1 subunit showed no signal. Pictures were taken on a Nikon TiE with a 40× Plan Fluor objective lens, with a cooled EMCCD camera and constant exposure time.

of 0.53 ± 0.06 mM and 7.25 ± 0.04 mM, respectively. In contrast, T1R1-372T/T1R3 showed comparable sensitivity to MSG with an EC_{50} value close to that of T1R1/T1R3 (0.19 ± 0.08 mM). Next, we examined the response to MSG of 2 T1R3 receptor variants coexpressed with T1R1. Dose–response curves for T1R1/T1R3-749S and T1R1/T1R3-757C showed that these variants with amino acid substitutions in the HTD (Figure 1) were severely impaired in their ability to respond to MSG leading to approximately 20% and 15% of the activation obtained with T1R1/T1R3 (EC_{50} values of 3.42 ± 0.05 mM and 11.2 ± 0.1 mM, respectively, Figure 4). Moreover, it should be pointed out that the EC_{50} values of these receptor variants are approximation because the concentration–response curves did not appear to reach saturation. Because differences in the activity of the functionally expressed receptors could be caused by dissimilarities in membrane targeting, immunostaining experiment was carried out using antibodies directed against T1R1 and T1R3 to verify the localization of the variant receptors in the plasma membrane. Although specific commercial antibodies generated against T1R3 are available, we found that antibodies against T1R1 are of poor quality (data not shown). For this reason, we developed rabbit polyclonal antibodies raised against hT1R1-VFT expressed in *E. coli*.
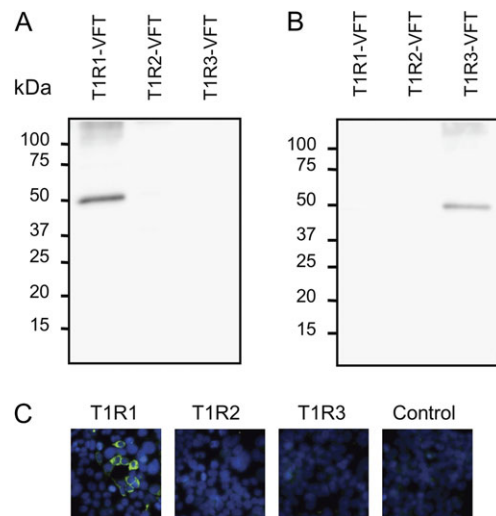
Western blotting analyses (Figure 5A) revealed a major immunoreactive band for T1R1-VFT migrating at approximatively 50 kDa, in agreement with its theoretical molecular weight, whereas T1R2- and T1R3-VFTs used as controls showed no signal. In control, commercial anti-T1R3 specifically labeled T1R3-VFT (Figure 5B). To provide more evidence that our anti-T1R1 antibodies specifically recognized the corresponding receptor protein, we performed immunohistochemistry analyses of HEK293/G16Gi3 cells expressing T1R1/T1R3, T1R2/T1R3, T1R3, or mock-transfected cells. As shown in Figure 5C, only T1R1 was detected, whereas T1R2 and T1R3 were not immunoreactive. Taken together, these results demonstrate that these antibodies are specific for T1R1 and T1R3 and may be used to study the expression of their variants in the plasma membrane.

As shown in Figure 6A, all 3 T1R1 variants and both T1R3 variants display a comparable staining pattern and similar level of expression (Figure 6B) although T1R3 appeared to be slightly more expressed than T1R1. Localization of receptors at the cell surface was then investigated using confocal microscopy. As shown in Figure 7, the immunofluorescence signal was mainly observed in the cytosol for
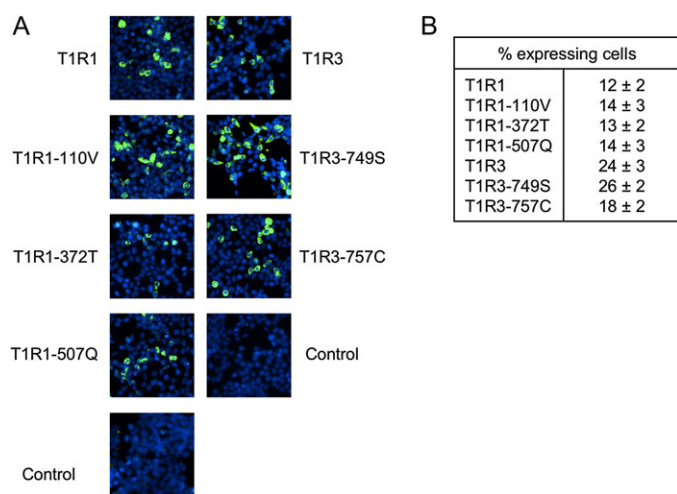
A

B

% expressing cells	
T1R1	12 ± 2
T1R1-110V	14 ± 3
T1R1-372T	13 ± 2
T1R1-507Q	14 ± 3
T1R3	24 ± 3
T1R3-749S	26 ± 2
T1R3-757C	18 ± 2

Figure 6 Cell-surface localization and expression rates of T1R1/T1R3 variants. **(A)** Immunocytochemistry of HEK293/G16Gi3 cells expressing T1R1/T1R3 variants. The T1Rs-expressing cells are shown in green, and nuclei are counterstained with DAPI (blue). The receptors were detected using a primary anti-T1R antibody and fluorescently labeled by a secondary Alexa-488–conjugated antibody. All data were obtained from the same transfection experiment. HEK293/G16Gi3 cells in the absence of T1R1/T1R3 receptor showed no signal with either antibody. Pictures were taken on a Nikon TiE with a 20× SFluor objective lens, with a cooled EMCCD camera and constant exposure time. **(B)** Percentage of cells expressing a given taste receptor variant. The expression rates were derived from 10 independent visual fields covering at least 350 cells and are given in percent ± standard deviation.

T1R1 and T1R3, whereas a small part of them could be detected at the cell surface. Nevertheless, these results demonstrated that both receptor variants have a similar subcellular distribution indicating that differences in MSG responses are not attributable to membrane targeting impairments.

To gain insight into the structural determinants of T1R1/T1R3 that might influence its function, we built homology VFT model using crystal structure of mGluR1 from the Protein Data Bank. The model was built in the active form A/closed-open with T1R3 open and T1R1 closed. T1R1 VFT was modeled with reference to the closed protomer (Kunishima et al. 2000) because this conformation of T1R1 allows to highlight the observed SNPs influence on the L-glutamate–binding pocket between lobe 1 (LB1) and lobe 2 (LB2) in active conformation.

Both mGluRs and T1R1 bind L-glutamate and their VFTs share ≈30% amino acid sequence identity and a highly similar arrangement of secondary structural elements. The Ramachandran plot of our model indicated that more than 98% of residues presented psi and phi angles in the core of allowed regions, and most bond lengths and angles were in the range of expected values (data not shown). Our model showed similarities with crystal structures of mGluRs, characterized by the typical VFT structure comprising 2 lobes LB1 and LB2 linked by a 3-stranded flexible hinge (Figure 8A). The 2 variant positions located in T1R1-VFT, A110V, and A372T, were observed in the lobe LB1

region, but interestingly, they are not involved in the L-glutamate–binding site. The A110 residue is involved in the interprotomer interface introducing hydrophobic interactions with residue K155 of T1R3 (data not shown) and its replacement by valine is likely to affect T1R1/T1R3 dimerization. The A372 residue is located in a large loop composed of 26 amino acid residues located near the entry of L-glutamate–binding cavity. The 3 other substitutions, T1R1-R507Q located in the CRR region T1R3-F749S and T1R3-R757C located in the HTD, cannot be observed in this model. Indeed, homology modeling cannot be easily used to model transmembrane domain because of the low identity of T1R1 and T1R3 with the few available structures (Palczewski et al. 2000; Cherezov et al. 2007). Besides, the CRR alignments with the only published template structure (Muto et al. 2007) did not allow an exploitable model (due to too high RMSD and many amino acids disallowed positions predicted in Ramachandran plot).

Automated docking of L-glutamate into the closed form of T1R1-VFT model revealed hydrogen bonds between the ligand and a group of residues located close to the hinge region linking LB1 and LB2 (residues R54, S148, T149, R151, S172, R249, and E301) and a cation–pi interaction with residue Y220 located in the ring of LB2 (Figure 8B). This is in agreement with the results by Zhang et al. (2008) who reported that L-glutamate docks in a similar binding position. The model was used to explore the effects of the amino acid substitutions on the 3D structure and L-glutamate docking. After superimposition of backbones of the T1R1-110V/T1R3 variant with T1R1/T1R3, we measured a 0.707 Å RMSD for the T1R1 backbone and 2.55 Å for the T1R3 backbone (Figure 9A). When comparing the T1R1/T1R3 dimer interface in wild-type and variant proteins, we found that this amino acid substitution did not lead to any major change in the LB2 interface (Figure 9B). However, we observed that 2 contact sites were modified in the LB1 interface corresponding to the environment of residues 110 and 180 (Figure 9B). These modifications induced significant conformational changes in the T1R3 monomer through an interface modification (K155 and R54 environment in T1R3) that might decrease the receptor functional activity. With regards to the A372T amino acid substitution, we observed a 0.320 Å RMSD with T1R1/T1R3 structure while the protomer interface was not significantly altered (data not shown). Figure 8C,D shows L-glutamate docking on A110V and A372T variants, respectively. It is worth noting that the position of L-glutamate in the T1R1-110V variant varies of 3.67 Å (corresponding to the RMSD calculation with T1R1) and of only 2.04 Å in the T1R1-372T variant. This difference of RMSD is clearly explained by the limited penetration of L-glutamate between T1R1 lobes 1 and 2 in T1R1-110V compared with T1R1-372T variant. In addition, we observed an overlap of the L-glutamate distal region (-CH2-CH2-COOH) docked in T1R1-372T variant that was not seen with T1R1. This distal region
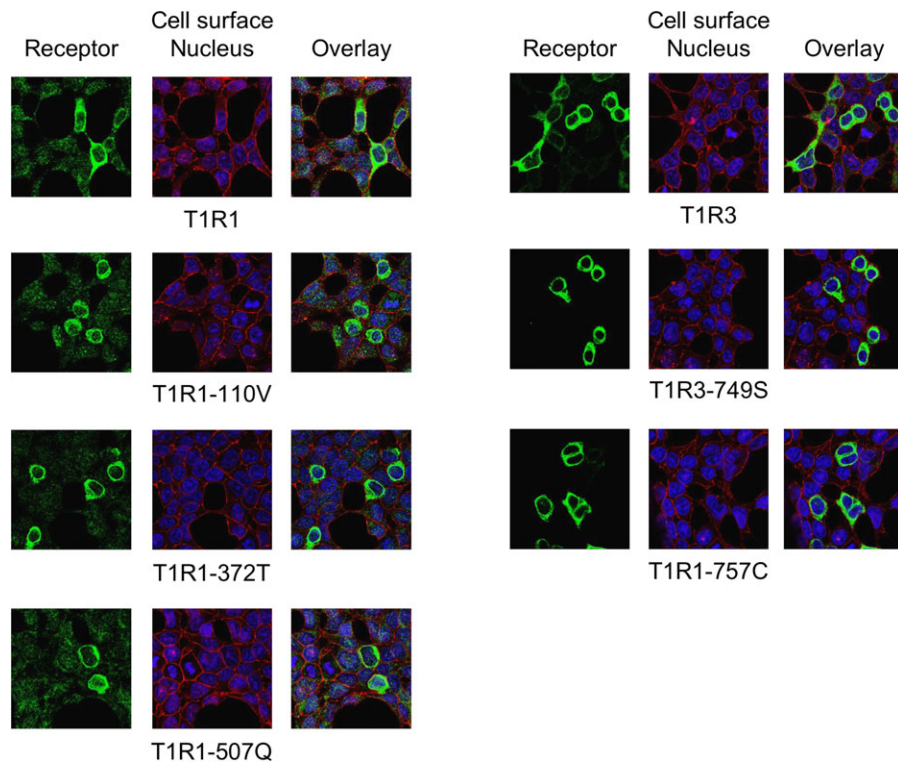
Figure 7 Cell-surface localization of HEK293/G16Gi3 cells were transiently transfected with plasmids expressing T1R1 and T1R3 and their variants. The cell surface (shown in red) is detected by biotin-conjugated concanavalin A and avidin-conjugated TRITC. Receptors (shown in green) were detected using primary antibody against T1R1 and T1R3 and revealed with fluorescent-labeled secondary antibody. A yellow color in the overlay images denotes a colocalization of the receptor with the cell surface. Figures were taken on Leica TCS SP2 AOBS confocal microscope with a 40× Plan Apo objective lens.

generates hydrogen bonds with the same amino acids (R151, R54, and R249). Moreover, residues E301 and R329 were involved in hydrogen bonds with the L-glutamate carboxylic and amino groups in the T1R1-372T variant. In the case of T1R1-110V variant, only 2 residues, E301 and R249, were involved in hydrogen bonds with L-glutamate. These results are in agreement with the calculated relative binding energy values: –10.61 kcal/mol for T1R1, –5.45 kcal/mol for the T1R1-110V variant, and –8.75 kcal/mol for T1R1-372T thus supporting the EC_{50} differences between receptor variants measured in calcium imaging experiments.

Discussion

In the present study, we looked at the correlation between in vivo and in vitro results of T1R1/T1R3 receptor activity when stimulated with MSG. Here, we confirm that the A110V, R507Q substitutions in T1R1 and F749S, R757C in T1R3, taken independently, lead to a reduced activity of T1R1/T1R3 expressed in HEK293 cells when stimulated by MSG, whereas A372T substitution in T1R1 did not reduce this activity. These data are in good agreement with Raliou, Wiencis, et al. (2009) who showed that A110V in T1R1 or R757C in T1R3 are statistically associated with impaired L-glutamate taste sensitivity in a sample of

Caucasian French population, whereas A372T in T1R1 is associated with normal sensitivity. The R507Q substitution in T1R1 also showed a trend to reduce sensitivity of the receptor in vivo. These results also corroborate the data from Shigemura, Shirosaki, Sanematsu, et al. (2009) who confirmed a reduced sensitivity associated with R757C in T1R3 using threshold evaluations in Japanese subjects as well as stimulation in vitro. Taken together with data from Chen et al. (2009) and Shigemura, Shirosaki, Sanematsu, et al. (2009), our results converge confirming a role of T1R1/T1R3 in the detection of L-glutamate.

T1R1 and T1R3 are members of the small family of class C GPCRs. Class C GPCRs possess in common a large VFT domain connected to a HTD typical of all GPCRs via a CRR. VFT domain of class C GPCR is implicated in ligand binding of conventional agonists and dimerization (Pin et al. 2004). Site-directed mutagenesis and molecular modeling have demonstrated that T1R1-VFT contains the binding sites of L-glutamate. The role of T1R3 in L-glutamate activation (Li et al. 2002; Zhang et al. 2008) is less clear. However, it has been demonstrated that T1R3 transmembrane domain binds the human sweet-taste inhibitor lactisole and the sweetener cyclamate. Although lactisole is able to inhibit activation of T1R1/T1R3 by L-glutamate, cyclamate does not activate the T1R1/T1R3 receptor by itself but
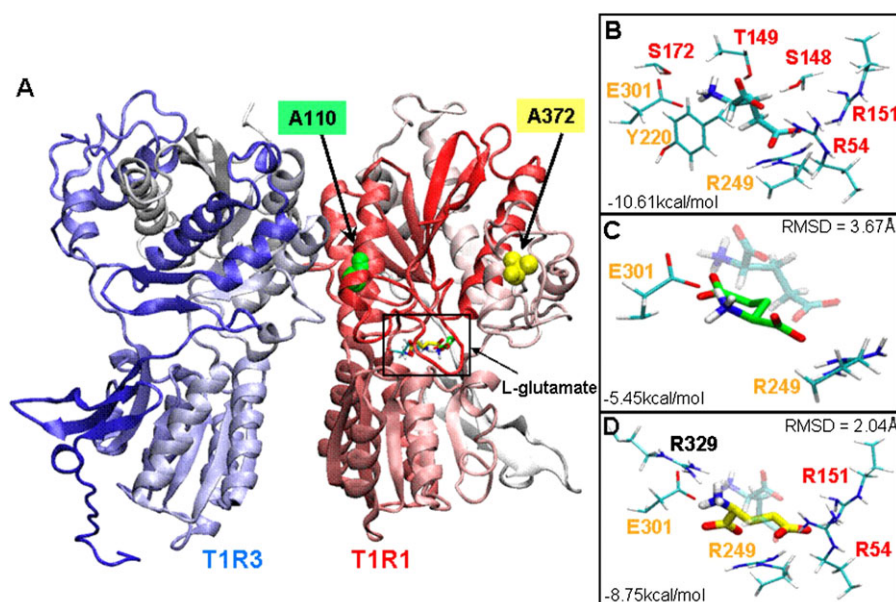
Figure 8 Molecular modeling of T1R1-T1R3 VFT dimer and ʟ-glutamate docking. **(A)** Molecular model of heterodimeric T1R1/T1R3 VFTs (red and blue, respectively). Variant positions in T1R1 corresponding to A110V and A372T are shown in green and yellow. The ʟ-glutamate–binding sites shown in boxes are located between LB1 and LB2. **(B)** Key residues for ʟ-glutamate (with blue C atom)–binding site docked in T1R1. **(C)** Key residues of T1R1-A110V variant for ʟ-glutamate docking, ʟ-glutamate C atom involved shown in green. **(D)** Key residues of T1R1-A372V variant for ʟ-glutamate docking, ʟ-glutamate C atom involved shown in yellow. Amino acid residues involved in ʟ-glutamate binding are labeled in red (LB1) and orange (LB2); the newly recruited amino acid residues are in black. Amino acid side chains and ʟ-glutamate are represented in thin and thick sticks, respectively. RMSD reported in boxes in C and D measures the difference between the ʟ-glutamate reference position in T1R1-VFT (B) and the variants. The relative binding energy value is indicated in kilocalorie per mole in each case.
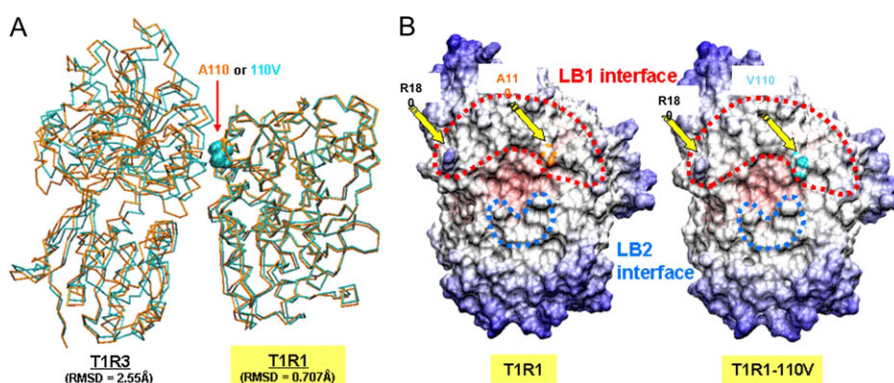

Figure 9 Dimer interfaces of T1R1/T1R3 variants. **(A)** Superimposed orthogonal views of T1R1/T1R3 in orange and T1R1-A110V/T1R3 in cyan. A110 in T1R1 and V110 in the variant are represented according to Van der Waals atoms. T1R1 and variants are superimposed with 0.707 Å RMSD and T1R3 with 2.55 Å. **(B)** Interaction surface of T1R1(s) representation (center to outside: red to blue). Broken lines red and blue represents interaction surface of dimer in LB1 and LB2 interface with T1R3, respectively. The major differences between T1R1 and T1R1-A110V variants are indicated by yellow arrows around residues 180 and 110.

potentiates the receptor response to ʟ-glutamate (Xu et al. 2004; Galindo-Cuspinera et al. 2006).

Although limited to the VFTs, we used 3D molecular modeling as a guide to explore the impact of the 110 and 372 amino acids replacements due to nsSNPs on T1R1/T1R3 receptor activity. In the resulting model, ʟ-glutamate was observed at a position analogous to that of the bound ʟ-glutamate both in the crystal structure of mGluR1 (Kunishima et al. 2000) and in the model of T1R1/T1R3

recently reported by Zhang et al. (2008), which was validated through site-directed mutagenesis. According to this model, the residue 110 is located at the T1R1/T1R3 dimer interface in T1R1-VFT introducing hydrophobic interactions with the T1R3 residue K155. The model suggests that the substitution of alanine by valine at this position may induce a large conformational change of the T1R1 monomer backbone. This could lead both to decrease the binding affinity for ʟ-glutamate and to disrupt the

contacts between subunits through surface modification. This latter event could be strong enough to affect the T1R3 conformation (Figure 9) and one could expect an incorrect recognition during the receptor dimerization, which may alter the activation process. The model suggests that both events likely contribute to the drastic loss of T1R1/T1R3 activity. Interestingly, the I60T polymorphism in the mouse T1R3 observed in saccharin nontaster strains has formerly also been predicted to affect dimerization between T1R2 and T1R3 (Max et al. 2001). However, it should be pointed out that Nie et al. (2005) showed that substitution reduces the affinity for ligands. The mutation T1R1-A110V could play a similar leading role for T1R1/T1R3.

Beyond the VFT domains, we also revealed that amino acid residue 507, located in T1R1 CRR is critical for umami receptor function. Multiple sequence alignment of this region in the family of class C GPCRs (data not shown) reveals that the T1R1 residue 507 fits with the conserved basic residue 519 (Muto et al. 2007). We can speculate that amino acid substitution at this position leads to the loss of a conserved negative charge and likely to a conformational change with a novel pairing of the neighboring disulphide bridges which could explain the loss of the receptor activity observed using the functional assay. Moreover, it has been shown that T1R3 CRR is an important determinant for the human T1R3 specific sensitivity to the sweet-tasting protein brazzein (Jiang et al. 2004).

As regard T1R3 amino acid substitutions tested, they also greatly affect the in vitro response to L-glutamate. Two of the nsSNPs detected in the French population (F749S and R757C), located in the intracellular domain showed inhibited response in vitro. The well-conserved phenylalanine in position 749 is located in transmembrane domain 5, where 2 residues important for lactisole binding have been identified (Jiang et al. 2004; Xu et al. 2004; Winnig et al. 2005). The arginine residue at position R757C is located in the intracellular loop 3, which seems important for G-protein coupling (Pin et al. 2004). Moreover, it should be noted that T1R3 was shown to poorly couple to G-proteins (Sainz et al. 2007). As expected, we found that both substitutions in this region strongly affect in vitro affinity of the receptor for L-glutamate. Comparing with the in vivo study, the R757C variation was significantly associated to nontasters, whereas the mutation at amino acid 749 was too seldom to lead to statistical evaluation. But grouping minor variants altogether led to statistical signification (Raliou, Wiencis, et al. 2009).

All together, molecular functional in vitro assays and 3D modeling of the genetic polymorphisms A110V, A372T, R507Q in T1R1, and R757C in T1R3 confirm the reported causal relations between the genotype and the psychophysical evaluation of interindividual differences of sensitivity to glutamate (phenotype). Moreover, this study also predicts that the rare F749S polymorphism should similarly impair the function of T1R1/T1R3 in vivo.

References

Bufe B, Breslin PA, Kuhn C, Reed DR, Tharp CD, Slack JP, Kim UK, Drayna D, Meyerhof W. 2005. The molecular basis of individual differences in phenylthiocarbamide and propylthiouracil bitterness perception. Curr Biol. 15:322–327.

Chaudhari N, Landin AM, Roper SD. 2000. A metabotropic glutamate receptor variant functions as a taste receptor. Nat Neurosci. 3:113–119.

Chaudhari N, Pereira E, Roper SD. 2009. Taste receptors for umami: the case for multiple receptors. Am J Clin Nutr. 90:738S–742S.

Chaudhari N, Yang H, Lamp C, Delay E, Cartford C, Than T, Roper S. 1996. The taste of monosodium glutamate: membrane receptors in taste buds. J Neurosci. 16:3817–3826.

Chen QY, Alarcon S, Tharp A, Ahmed OM, Estrella NL, Greene TA, Rucker J, Breslin PA. 2009. Perceptual variation in umami taste and polymorphisms in TAS1R taste receptor genes. Am J Clin Nutr. 90:770S–779S.

Cherezov V, Rosenbaum DM, Hanson MA, Rasmussen SG, Thian FS, Kobilka TS, Choi HJ, Kuhn P, Weis WI, Kobilka BK, et al. 2007. High-resolution crystal structure of an engineered human β2-adrenergic G protein-coupled receptor. Science. 318:1258–1265.

Combet C, Blanchet C, Geourjon C, Deléage G. 2000. NPS@: Network Protein Sequence Analysis. Trends Biochem Sci. 25:147–150.

Damak S, Rong M, Yasumatsu K, Kokrashvili Z, Varadarajan V, Zou S, Jiang P, Ninomiya Y, Margolskee RF. 2003. Detection of sweet and umami taste in the absence of taste receptor T1r3. Science. 301:850–853.

Drayna D, Coon H, Kim UK, Elsner T, Cromer K, Otterud B, Baird L, Peiffer AP, Leppert M. 2003. Genetic analysis of a complex trait in the Utah Genetic Reference Project: a major locus for PTC taste ability on chromosome 7q and a secondary locus on chromosome 16p. Hum Genet. 112:567–572.

Fuller JL. 1974. Single-locus control of saccharin preference in mice. J Hered. 65:33–36.

Galindo-Cuspinera V, Breslin PA. 2006. The liaison of sweet and savory. Chem Senses. 31:221–225.

Galindo-Cuspinera V, Winnig M, Bufe B, Meyerhof W, Breslin PA. 2006. A TAS1R receptor-based explanation of sweet "water-taste". Nature. 441:354–357.

Huang XQ, Hardison RC, Miller W. 1990. A space-efficient algorithm for local similarities. Comput Appl Biosci. 6:373–381.

Humphrey W, Dalke A, Schulten K. 1996. VMD: visual molecular dynamics. J Mol Graph. 14:33–3827–28.

Jiang P, Ji Q, Liu Z, Snyder LA, Benard LM, Margolskee RF, Max M. 2004. The cysteine-rich region of T1R3 determines responses to intensely sweet proteins. J Biol Chem. 279:45068–45075.

Kim UK, Wooding S, Riaz N, Jorde LB, Drayna D. 2006. Variation in the human TAS1R taste receptor genes. Chem Senses. 31:599–611.

Kuninaka A. 1960. Studies on taste of nucleic acid derivatives. J Agric Chem Soc Jnp. 34:487–492.

Kuninaka A, Kibi M, Sakaguchi K. 1964. History and development of flavor nucleotides. Food Technol. 18:29.

Kunishima N, Shimada Y, Tsuji Y, Sato T, Yamamoto M, Kumasaka T, Nakanishi S, Jingami H, Morikawa K. 2000. Structural basis of glutamate recognition by a dimeric metabotropic glutamate receptor. Nature. 407:971–977.

Laskowski RA, Rullmann JA, MacArthur MW, Kaptein R, Thornton JM. 1996. AQUA and PROCHECK-NMR: programs for checking the quality of protein structures solved by NMR. J Biomol NMR. 8:477–486.

Li X, Staszewski L, Xu H, Durick K, Zoller M, Adler E. 2002. Human receptors for sweet and umami taste. Proc Natl Acad Sci U S A. 99:4692–4696.

Lugaz O, Pillias AM, Faurion A. 2002. A new specific ageusia: some humans cannot taste L-glutamate. Chem Senses. 27:105–115.

Lush IE. 1989. The genetics of tasting in mice. VI Saccharin, acesulfame, dulcin and sucrose. Genet Res. 53:95–99.

Maruyama Y, Pereira E, Margolskee RF, Chaudhari N, Roper SD. 2006. Umami responses in mouse taste cells indicate more than one receptor. J Neurosci. 26:2227–2234.

Max M, Shanker YG, Huang L, Rong M, Liu Z, Campagne F, Weinstein H, Damak S, Margolskee RF. 2001. Tas1r3, encoding a new candidate taste receptor, is allelic to the sweet responsiveness locus Sac. Nat Genet. 28:58–63.

Muto T, Tsuchiya D, Morikawa K, Jingami H. 2007. Structures of the extracellular regions of the group II/III metabotropic glutamate receptors. Proc Natl Acad Sci U S A. 104:3759–3764.

Nelson G, Chandrashekar J, Hoon MA, Feng L, Zhao G, Ryba NJ, Zuker CS. 2002. An amino-acid taste receptor. Nature. 416:199–202.

Nelson G, Hoon MA, Chandrashekar J, Zhang Y, Ryba NJ, Zuker CS. 2001. Mammalian sweet taste receptors. Cell. 106:381–390.

Nie Y, Vigues S, Hobbs JR, Conn GL, Munger SD. 2005. Distinct contributions of T1R2 and T1R3 taste receptor subunits to the detection of sweet stimuli. Curr Biol. 15:1948–1952.

Palczewski K, Kumasaka T, Hori T, Behnke CA, Motoshima H, Fox BA, Le Trong I, Teller DC, Okada T, Stenkamp RE, et al. 2000. Crystal Structure of Rhodopsin: A G Protein-Coupled Receptor. Science. 289:739–745.

Phillips JC, Braun R, Wang W, Gumbart J, Tajkhorshid E, Villa E, Chipot C, Skeel RD, Kalé L, Schulten K. 2005. Scalable molecular dynamics with NAMD. J Comput Chem. 26:1781–1802.

Pin JP, Kniazeff J, Goudet C, Bessis AS, Liu J, Galvez T, Acher F, Rondard P, Prézeau L. 2004. The activation mechanism of class-C G-protein coupled receptors. Biol Cell. 96:335–342.

Raliou M, Boucher Y, Wiencis A, Bézirard V, Pernollet JC, Trotier D, Faurion A, Montmayeur JP. 2009. Tas1R1-Tas1R3 taste receptor variants in human fungiform papillae. Neurosci Lett. 451:217–221.

Raliou M, Wiencis A, Pillias AM, Planchais A, Eloit C, Boucher Y, Trotier D, Montmayeur JP, Faurion A. 2009. Nonsynonymous single nucleotide polymorphisms in human tas1r1, tas1r3, and mGluR1 and individual taste sensitivity to glutamate. Am J Clin Nutr. 90:789S–799S.

Reed DR, Li S, Li X, Huang L, Tordoff MG, Starling-Roney R, Taniguchi K, West DB, Ohmen JD, Beauchamp GK, et al. 2004. Polymorphisms in the taste receptor gene (Tas1r3) region are associated with saccharin preference in 30 mouse strains. J Neurosci. 24:938–946.

Sainz E, Cavenagh MM, Lopez Jimenez ND, Gutierrez JC, Battey JF, Northup JK, Sullivan SL. 2007. The G-protein coupling properties of the human sweet and amino acid taste receptors. Dev Neurobiol. 67:948–959.

Sali A, Blundell TL. 1993. Comparative protein modelling by satisfaction of spatial restraints. J Mol Biol. 234:779–815.

San Gabriel A, Maekawa T, Uneyama H, Torii K. 2009. Metabotropic glutamate receptor type 1 in taste tissue. Am J Clin Nutr. 90: 743S–746S.

San Gabriel A, Uneyama H, Yoshie S, Torii K. 2005. Cloning and characterization of a novel mGlur1 variant from vallate papillae that functions as a receptor for L-glutamate stimuli. Chem Senses. (30 Suppl) 1:i25–i26.

Sanner MF. 2005. A component-based software environment for visualizing large macromolecular assemblies. Structure. 13:447–462.

Shi J, Blundell TL, Mizuguchi K. 2001. FUGUE: sequence-structure homology recognition using environment-specific substitution tables and structure-dependent gap penalties. J Mol Biol. 310:243–257.

Shigemura N, Shirosaki S, Ohkuri T, Sanematsu K, Islam AS, Ogiwara Y, Kawai M, Yoshida R, Ninomiya Y. 2009. Variation in umami perception and in candidate genes for the umami receptor in mice and humans. Am J Clin Nutr. 90:764S–769S.

Shigemura N, Shirosaki S, Sanematsu K, Yoshida R, Ninomiya Y. 2009. Genetic and molecular basis of individual differences in human umami taste perception. PLoS One. 4:e6717.

Toyono T, Seta Y, Kataoka S, Harada H, Morotomi T, Kawano S, Shigemoto R, Toyoshima K. 2002. Expression of the metabotropic glutamate receptor, mGluR4a, in the taste hairs of taste buds in rat gustatory papillae. Arch Histol Cytol. 65:91–96.

Winnig M, Bufe B, Meyerhof W. 2005. Valine 738 and lysine 735 in the fifth transmembrane domain of rTas1r3 mediate insensitivity towards lactisole of the rat sweet taste receptor. BMC Neurosci. 6:22.

Xu H, Staszewski L, Tang H, Adler E, Zoller M, Li X. 2004. Different functional roles of T1R subunits in the heteromeric taste receptors. Proc Natl Acad Sci U S A. 101:14258–63.

Yamaguchi S. 1991. Basic properties of umami and effects on humans. Physiol Behav. 49:833–841.

Yang H, Wanner IB, Roper SD, Chaudhari N. 1999. An optimized method for in situ hybridization with signal amplification that allows the detection of rare mRNAs. J Histochem Cytochem. 47:431–446.

Zhang F, Klebansky B, Fine RM, Xu H, Pronin A, Liu H, Tachdjian C, Li X. 2008. Molecular mechanism for the umami taste synergism. Proc Natl Acad Sci U S A. 105:20930–20934.

Zhao GQ, Zhang Y, Hoon MA, Chandrashekar J, Erlenbach I, Ryba NJ, Zuker CS. 2003. The receptors for mammalian sweet and umami taste. Cell. 115:255–266.